J Appl Electrochem (2008) 38:605–612
DOI 10.1007/s10800-007-9478-y

ORIGINAL PAPER

# Influence of cathodic overpotential on grain size in nanocrystalline nickel deposition on rotating cylinder electrodes

**E. Moti' · M. H. Shariat · M. E. Bahrololoom**

Received: 30 March 2007 / Revised: 17 December 2007 / Accepted: 26 December 2007 / Published online: 12 January 2008


**Abstract** Nanocrystalline (nc) nickel was electrodeposited using rotating cylindrical electrodes (RCD) from a Watt's bath containing saccharin. The effects of cathode rotation speed and saccharin concentration on the cathodic overpotential and grain size were studied. The grain sizes are presented as a function of the cathodic overpotential. All reported cathodic overpotentials were corrected for ohmic overpotentials. X-ray diffraction (XRD) and transmission electron microscopy (TEM) were used to determine the deposit grain size. In addition, the influences of cathode rotation speed and current density on the morphology of nanocrystalline nickel were observed by scanning electron microscopy (SEM).

**Keywords** Cathodic overpotential · Electrodeposition · Grain size · Nanocrystalline · Nickel · Rotating cylindrical electrode

## 1 Introduction

In the last two decades, as a result of advances in the understanding of the effects of grain size on the properties of materials, structures with grain sizes less than 100 nm (nc materials) have received considerable attention. Nc materials can be made by approaches like inert gas condensation, electrodeposition, ball milling and severe plastic deformation [1]. Efforts have been made to synthesize nc Ni [2], Co [3], Zn [4], Ni–Co [5], Ni–B [6], Ni–Zn [7], Ni–WC [8], and Ni–SiC [9] by electrodeposition due to the economical and technological advantages of this method [10].

In electrodeposition, nucleation and growth are in competition to determine grain size. Therefore, high nucleation rates and low growth rates are unavoidable for the electrodeposition of nc materials. Cathodic overpotential has been suggested as an important factor in fine grain deposition [11, 12]. Based on the Glasstone relation [13], the activation energy of nucleation ($A_k$) is influenced by absolute cathodic overpotential ($\eta$), the activity of the metallic ion on the cathode film ($a'_{Me^+}$), and the activity of the metallic ion in the bulk of the solution ($a_{Me^+}$).

$$A_k \propto \left\{ \frac{1}{[\eta + (a'_{Me^+}/a_{Me^+})^2]} \right\} \quad (1)$$

Some additives in aqueous electrodeposition solutions are known to change the cathodic overpotential and the grain size [14–17]. For example, the addition of polyacrylamide and thiourea to a Watt's bath decreases cathodic overpotential (about 10 mV) and refines the grains [17]. The advantages of pulse current, which include better additive adsorption and higher metallic ion concentration on the cathode surface were used to deposit nc metals [3, 18]. Therefore, ideal conditions for nano grain production are high-negative overpotential, high-adion population and low-adion surface mobility [11].

Rotating electrodes have been used since 1905 for the electrodeposition of pure metals, alloys and metal matrix composites [19–21]. Details of hydrodynamics, mass transport and fundamental characteristics of rotating cylindrical electrodes are available elsewhere [21]. In general, the rotating electrode has established new opportunities for electrochemical techniques based on uniform potential, current distribution, and high mass transport [21]. Nc nickel

E. Moti' · M. H. Shariat (✉) · M. E. Bahrololoom
Department of Materials Science and Engineering, School of Engineering, Shiraz University, Shiraz 71348-15939, Iran
e-mail: shariat@shirazu.ac.ir

was electrodeposited at a rotating disk electrode in sulfamate solution [22]. While there is evidence highlighting the effects of cathode movement on cathodic overpotential [23], there has been no work featuring the effects of cathodic overpotential on the grain size.

In this paper, some electrochemical aspects of electrodeposition of nc nickel produced by a novel method are presented. The effects of cathode rotation speed and saccharin concentration on cathodic overpotential, grain size, texture and morphology are discussed. A quantitative relation between cathodic overpotential and grain size is presented.

## 2 Experimental

Cylindrical copper cathodes (15 mm diameter) of two different surface areas (1 and 10 $cm^2$) were used as substrates for the electrodeposition of nc nickel (35–100 μm thickness) using a direct current (2–22 A $dm^{-2}$) and 0–800 rpm rotation speeds. A Watts bath containing $NiSO_4 \cdot 6H_2O$ (300 g $L^{-1}$), $NiCl_2 \cdot 6H_2O$ (45 g $L^{-1}$) and $H_3BO_3$ (45 g $L^{-1}$) was used with the addition of saccharin (0–5 g $L^{-1}$) as a grain refiner, and sodium lauryl sulphate (0.25 g $L^{-1}$) as an anti-pitting agent (all analytical grade chemicals). The bath temperature was adjusted at 60 ± 1 °C. Before plating, the substrates were degreased with acetone and then electropolished by dipping into a solution containing 25 vol% phosphoric acid (33 wt%), 25 vol% ethanol alcohol (99 vol%), and 50 vol% distilled water, while applying a 10–15 A $dm^{-2}$ current density for 1 min at room temperature. The anodes were two nickel sheets (total surface area 45 $cm^2$) fixed on two sides of the cathode at a 2 cm distance. The pH was 2, and was kept constant by adding a mixture (7:1) of $H_2SO_4$ (98 wt%):HCl (36 wt%) to the bath. The electrolytes were replaced after coating five specimens. Conductivity was measured for the bath at different saccharin concentrations using a KARL KOLB conductivity probe at 60 ± 1 °C. An Ecochemi Auto Lab potentiostat/galvanostat was used to control the current and to monitor the corresponding voltage. The current and voltage measurements were recorded using a computer-based data acquisition system. A calomel electrode was placed at a 6 mm distance from the cathode.

The microstructures of deposits were characterized by D8 Bruker X-ray diffraction (XRD). The X-ray scan rate was 0.05° $s^{-1}$ with Cu Kα radiation ($\lambda = 0.15405$ nm). The grain size was determined from X-ray peak broadening by applying the Scherrer formula for (100) reflections [24]. The peak broadenings were measured by the integral width method [24] and corrected for instrumental peak broadening using a full annealed nickel (at 600 °C for 24 h) by the Jones equation [24]. To verify the accuracy of the grain size measurements, some specimens were also examined in a C.M. 200-S.E.G. Philips scanning transmission electron microscope (STEM). For TEM specimens, samples were prepared by jet polishing with a 10 vol% perchloric acid, 15 vol% acetic acid, and 75 vol% methanol electrolyte at −20 °C and an applied voltage of 20 V. The grain size of nc nickel was determined directly from dark-field and bright-field transmission electron micrographs by measuring 120 grains. Morphological studies of deposits were carried out using an Oxford Instruments Stereoscan 120 scanning electron microscope (SEM). The current efficiency was calculated from the current passed and the weight gained by applying Faraday's law.

## 3 Results and discussion

### 3.1 SEM studies

Figure 1a and b show the morphology of bright nickel deposited at 2 A $dm^{-2}$ and 5 g $L^{-1}$ saccharin concentration with a stationary cathode at two different magnifications. The deposit exhibits areas which have two different morphologies. With higher magnifications, pyramids are observed in the darker parts. Such a rough morphology was related to matt nickel deposits with large grains that are deposited without the addition of grain refiner to the bath [3]. On the other hand, there are sections having a smooth morphology which is similar to that of finer grain deposits shown in Fig. 1c. Smooth morphology, as well as colony-like morphology, have been reported for nanocrystalline nickel deposits because of pyramidal growth inhibition by incorporated organic additives [3, 25]. Apparently, on a stationary cathode saccharin cannot be adsorbed uniformly on the cathode surface. Consequently, in some areas grain refining was disrupted and pyramidal growth occurred. In contrast, as a result of more uniform saccharin adsorption on the rotating cylinder electrode, a more uniform and smoother nickel deposit than that at a stationary cathode was observed (Fig. 1c). Figure 1d shows the bumpy morphology of nickel deposited on the rotating cathode with a rotation speed of 800 rpm. This type of morphology can be attributed to the shearing and adsorption forces resulting in saccharin adsorption disruption. Similar behaviour was reported for the incorporation of ceramic particles in composite electrodeposition [23].

### 3.2 TEM studies

Figure 2 shows typical planer bright-field STEM micrographs for an nc nickel deposit produced from a bath containing 5 g $L^{-1}$ saccharin at 2 A $dm^{-2}$ and 500 rpm. The grain size distribution is in the range 8–25 nm, and the

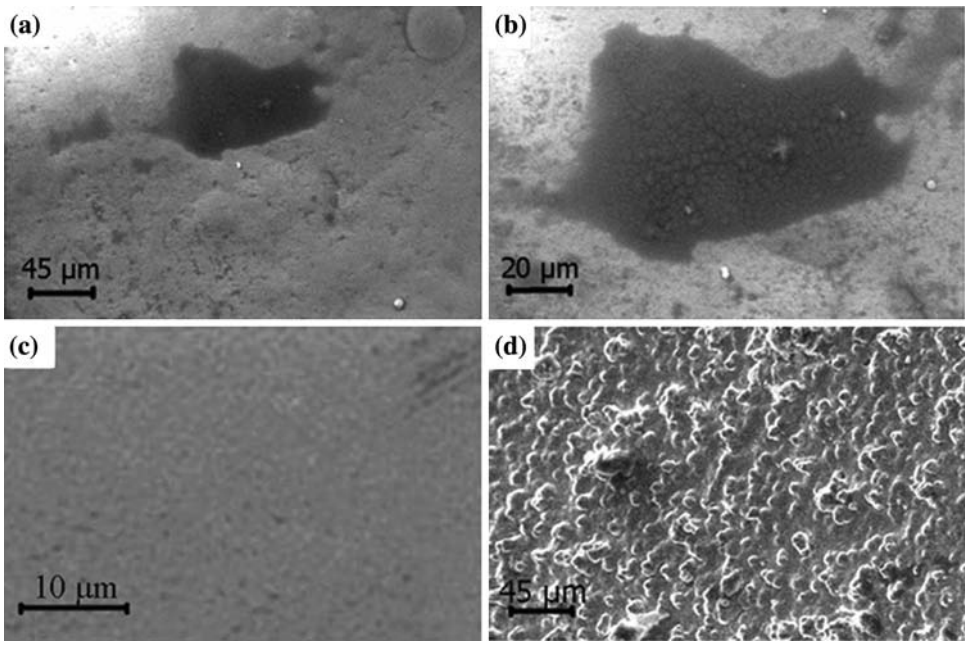


**Fig. 1** The influences of cathode rotation speed on the morphology of nickel deposits at 2 A $dm^{-2}$ and saccharin concentration 5 g $L^{-1}$. (**a** and **b**) stationary cathode, (**c**) 500 rpm and (**d**) 800 rpm

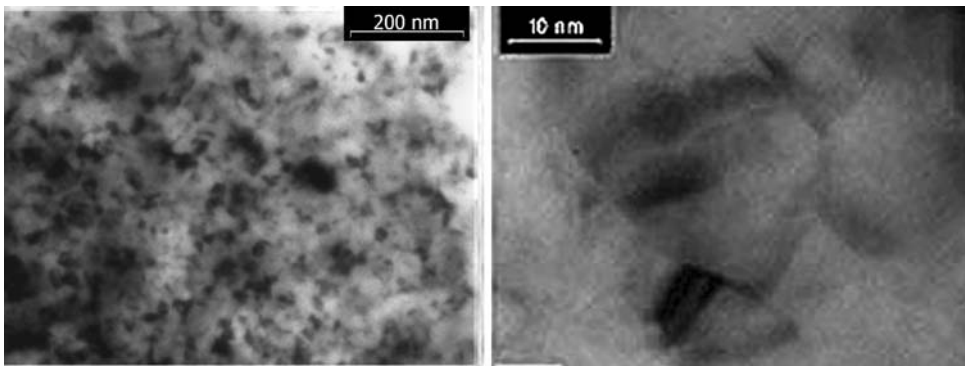


**Fig. 2** Scanning transmission electron micrographs of nanocrystalline Ni, electrodeposited with bath containing 5 g $L^{-1}$ saccharin, 2 A $dm^{-2}$, 500 rpm including bright-field views in the plane of the foil

determined average grain size is 13.5 nm, which is in good agreement with the XRD results. This consistency implies that the XRD technique is a suitable method to characterize the grain size of nc nickel in this study. Like the planer micrographs of nc nickel, which was electrodeposited by the DC current technique [26], an equiaxed grain structure was observed, as shown in the TEM micrographs of Fig. 3. Such microstructures have been reported by El-Sherik and Erb [3].

### 3.3 Ohmic overpotential

The measured potential at the cathode appears more negative than it should be due to the effect of ohmic losses. Therefore, all measured overpotentials were corrected by subtracting the IR drop from the cathodic overpotential. The solution resistance R (Ω), which is a small amount in aqueous solutions, can be calculated accurately enough in a concentric cylinder configuration according to [27]

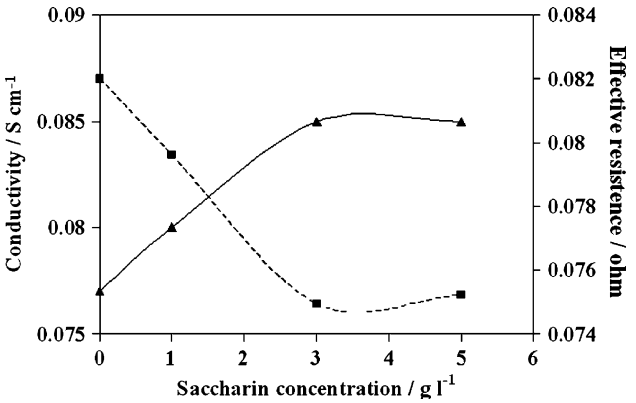


**Fig. 3** Effect of saccharin concentration on conductivity (-■-) and effective resistance (-▲-) of the bath

$$R = \frac{1}{2\pi kh}\ln\left(\frac{r_0}{r}\right) \quad (2)$$

where $r_0$ is the inner radius of the outer cylinder (the location of the reference electrode), $r$ is the outer radius of

the inner cylinder, $k$ (S cm$^{-1}$) is the conductivity of the solution, and $h$ (cm) the height of the solution (assumed to be the same as the height of the cathode). Conductivity and solution resistance as a function of saccharin concentration are shown in Fig. 3. The conductivity of the plating bath is not affected significantly by the saccharin concentration. A slight decrease in solution conductivity can be due to the negligible interaction between saccharin ions and nickel ions in the solution.

### 3.4 Effect of saccharin concentration on cathodic overpotential and grain size

Figure 4 shows that increasing saccharin concentration diminishes cathodic overpotential and grain size at 2 A dm$^{-2}$ and 500 rpm. Grain sizes were decreased from a few micrometers size in the bath without saccharin to 14 nm at 5 g L$^{-1}$ saccharin concentration. There are two viewpoints related to the effect of saccharin on grain size. Saccharin increases the nucleation rate by increasing the absolute cathodic overpotential as well as inhibiting growth [3, 28]. Saccharin is slightly acidic in aqueous solutions [29]. It is dissolved in aqueous solutions by dissociation of the N–H bands and hydration of the saccharin anion. [29]. Therefore, the addition of saccharin to a Watts bath changes the composition of the Helmholtz layer so that changes of cathodic overpotential are expected. As a result of the increase in the absolute amount of cathodic overpotential, the nucleation rate is increased and grain size is diminished [13, 30]. On the other hand, the saccharin anions can be adsorbed on active growth sites on the cathode and produce transient chemical or physical barrier layers to transport adions and adatoms on the cathode surface and so inhibit growth.

### 3.5 Effect of cathode rotation speed on cathodic overpotential and grain size

The effects of cathode rotation speed on cathodic overpotential and grain size are shown in Fig. 5. The absolute values of cathodic overpotential were increased by about 35 mV for an increase in cathode rotation speed up to 500 rpm. In contrast, at rotation speeds of more than 500 rpm the absolute cathodic overpotential was decreased.

After subtracting the resistive overpotential, the overvoltage of an individual electrode may be expressed as the sum of contributions from activation and concentration overvoltages [31]. Although a decrease in the absolute cathodic overpotential is expected due to cathode rotation resulting a high mass transport rate, an increase in absolute cathodic overpotential was clearly observed up to 500 rpm. This discrepancy indicates that the major part of cathodic overpotential is activation overpotential, which is affected by saccharin adsorption on the cathode surface. Therefore, cathode rotation can create better conditions for saccharin to act as a more effective grain refiner. The decrease in absolute cathodic overpotential at cathode rotation speeds of more than 500 rpm can be attributed to shearing and adsorption forces. Saccharin anions that can interact with nickel ions are large ions, so saccharin adsorption can be disrupted at high cathode rotation speeds. Similar behaviour was reported for the adsorption of polymeric particles on the cathode surface for composite electrodeposition [32].

### 3.6 Effect of current density on cathodic overpotential and morphology

The effect of current density on the cathodic overpotential at 5 g L$^{-1}$ saccharin and 500 rpm is presented in Fig. 6a.

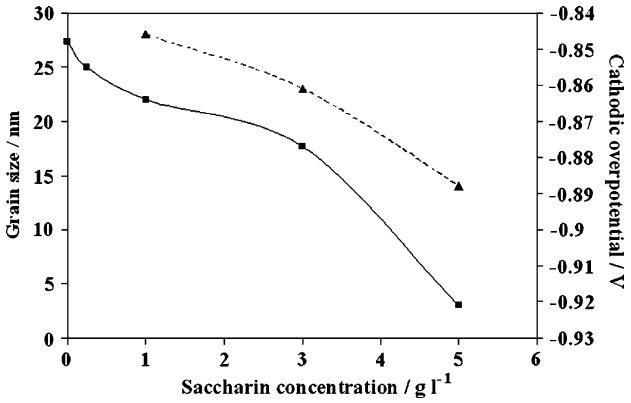


**Fig. 4** Effect of saccharin concentration on cathodic overpotential (-■-) and grain size (-▲-) in 2 A dm$^{-2}$ and 500 rpm

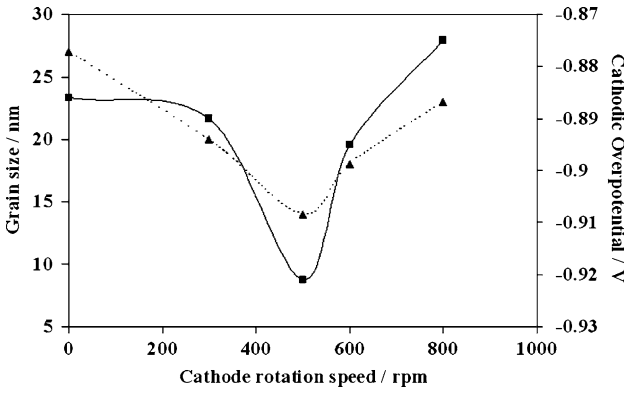


**Fig. 5** Effect of cathode rotation speed on cathodic overpotential (-■-) and grain size (-▲-) at 2 A dm$^{-2}$ and 5 g L$^{-1}$ saccharin concentration

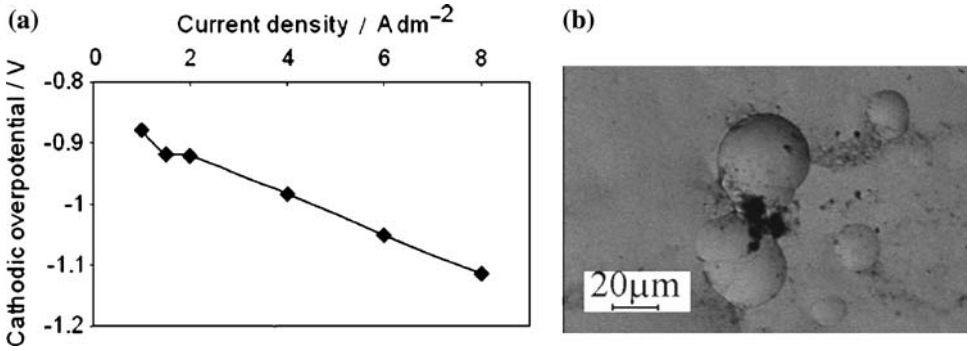


**Fig. 6** (**a**) Effect of current density on the cathodic overpotential at 500 rpm and 5 g $L^{-1}$ saccharin concentration. (**b**) Morphology of nickel deposit at 6 A $dm^{-2}$, 500 rpm and 5 g $L^{-1}$ saccharin concentration

Although the limiting current density cannot be calculated using this figure, it is known that increase in current density increases the absolute cathodic overpotential. The morphology of a nickel deposited at 6 A $dm^{-2}$, 500 rpm and 5 g $L^{-1}$ saccharin concentration is shown in Fig. 6b. Some blisters are observed as a result of the adsorbed hydrogen. Because of the large amount of hydrogen absorption or hydrogen evolution, the pH can increase locally. Therefore, the black areas in Fig. 6b may be nickel hydroxide. In addition, pH increases were more clearly observed in electrodeposition at high current densities (4–22 A $dm^{-2}$) and 5 g $L^{-1}$ saccharin. This could prove the reduction of hydrogen ions as a result of concentration overpotential in this condition.

### 3.7 XRD studies

Some X-ray diffractograms measured at different cathode rotation speeds at 2 A $dm^{-2}$ and 5 g $L^{-1}$ saccharin are shown in Fig. 7. As a result of the thinner coating, X-ray reflections, marked S, originating from the substrate, are seen in Fig. 7b. Textural changes were observed in Fig. 7. The intensity ratio $R_I = I(200)/I(111)$ is decreased by increasing the cathode rotation speed. This is related to greater adsorption of saccharin ions or atomic hydrogen on the cathode surface during electrodeposition [33]. Nickel deposits in the presence of an organic additive had (111) texture or an apparently random orientation [34]. In addition, it was reported that, by using a rotating electrode, hydrogen reduction on the cathode is increased and in turn inhibits growth in the (200) direction [35]. Both reports agree with the XRD results in this work.

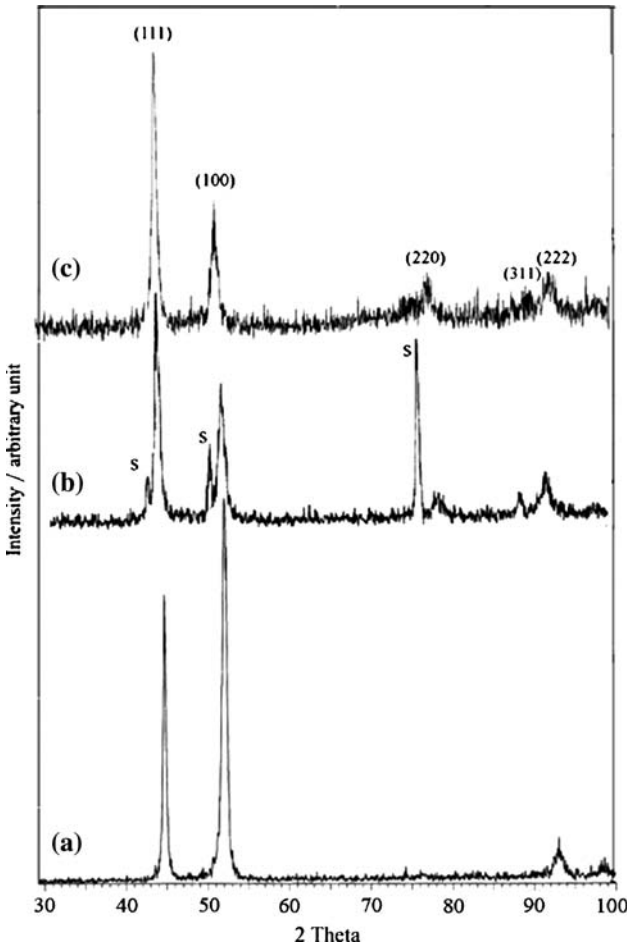


**Fig. 7** X-ray diffraction pattern for nickel at different cathode rotation speed, (**a**) stationary cathode, (**b**) 500 and (**c**) 800 rpm at 5 g $L^{-1}$ saccharin concentration and 2 A $dm^{-2}$

## 4 Electrodeposited grain size model

The use of RCE is known to refine the grain size of the electrodeposited coatings. In electrodeposition the new phase formation has to surmount an energy barrier related to the accumulation of initial atoms to form clusters sufficiently stable to give birth to the new phase. According to the classical theory on electrochemical phase formation and growth, the two dimensional (2D) nucleation rate, $J$ ($m^{-2}$ $s^{-1}$) is given by [30],

$$J = k_{2d}\exp\left(\frac{-bS\varepsilon^2}{zekT\eta}\right) \quad (3)$$

where, $k_{2d}$ ($m^{-2}$ $s^{-1}$) is the rate constant, $b$is the geometric factor depending on the shape of the 2D cluster

(dimensionless), $S$ the area occupied by one atom on the surface of the cluster ($m^2$), $\varepsilon$ the specific edge energy (J $m^{-1}$), $z$ the electronic charge of an ion (dimensionless), $e$ the charge of an electron (C), $k$ the Boltzmann constant (J $K^{-1}$), and $\eta$ the overpotential (V). Assuming that the value of $\frac{bS\varepsilon^2}{zekT}$ is constant and equal to $Q_{2d}$ ($V$), Eq. 3 can be rewritten in the form

$$J_{2d} = k_{2d} \exp\left(-\frac{Q_{2d}}{\eta}\right) \tag{4}$$

The number of grains (assuming that the grain shape is spherical), $N_0$ ($m^{-2}$), is equal to the product of nucleation rate ($J$), the electrodeposition time ($t$) and the cathode area ($A$), i. e.

$$N_0 = J_{2d} t A \tag{5}$$

Substituting $J$ from Eq. 4 into Eq. 5, the expression for $N_0$ is

$$N_0 = k_{2d} t A \exp\left(-\frac{Q_{2d}}{\eta}\right) \tag{6}$$

The average grain volume $G_V$ ($m^3$) is equal to the total volume of deposit $V$ ($m^3$), divided by the number of grains, $N_0$. The volume of the deposit can be calculated by Faraday's law and the current efficiency mentioned in Table 1. In addition, $G_V$, $V$, $\eta$, $t$, $A$ and some electrodeposition conditions are presented in Table 1.

$$G_V = \frac{V}{N_0} \tag{7}$$

which can be rewritten as

$$G_V = \frac{V}{k_{2d} t A \exp\left(-\frac{Q_{2d}}{\eta}\right)} \tag{8}$$

$$Lnk_{2d} - \frac{Q_{2d}}{\eta} = Ln\frac{V}{G_V t A} \tag{9}$$

By a similar method from Eq. 10 [34], the relation between the three dimensional rate constant ($k_{3d}$) and the activation potential of three dimensional nucleation ($Q_{3d}$) was extracted (Eq. 11).

$$J_{3d} = k_{3d} \exp\left(-\frac{Q_{3d}^2}{\eta^2}\right) \tag{10}$$

$$Lnk_{3d} - \frac{Q_{3d}^2}{\eta^2} = \ln\frac{V}{G_V t A} \tag{11}$$

where $J_{3d}$ is the three dimensional nucleation rate, $G_V$ is the grain volume, and $V$ the total volume of the deposit.

Figure 8 shows the relation between $Ln\frac{V}{G_A t A}$ and the reciprocal of cathodic overpotential, while Fig. 9 shows the relation between $Ln\frac{V}{G_V t A}$ and the square reciprocal of the cathodic overpotential. Three kinds of points are exhibited in these figures. First, lozenge-like points (◆) with coordinates extracted from nickel electrodeposition at different cathode rotation speeds. Second, circular points (●) with coordinates calculated from nickel electrodeposition at different saccharin concentrations at a constant cathode rotation speed and, finally, a triangular (▲) point with coordinates computed from data for nickel electrodeposition on stationary cathodes in the bath containing saccharin. In these two figures, the trendlines were calculated with circular (●) and lozenge (◆) points. The trendlines are accurate lines through these points because their linear type $R$-squared values (0.9711 and 0.9707) approach 1. The circular points (●) have more conformity with the trendlines compared with the Lozenge points (◆). Therefore, for a fixed cathode rotation speed, the cathodic overpotential that was controlled by the saccharin concentration (1–5 g $L^{-1}$) clearly satisfied these models. In addition, in this condition $bS\varepsilon^2$and probably $b$, $S$ and $\varepsilon^2$ are constants. On the other hand, because of a small deviation from the model at different cathode rotation speeds and 5 g $L^{-1}$ saccharin, the amount of $bS\varepsilon^2$ is changed. This is due to the hydrogen adsorption change with the cathode rotation speed [35]. The triangular point for the stationary cathode, clearly deviates from the trendline. This may be a result of the significant influence of cathode rotation on hydrogen

**Table 1** Electrodeposition parameters and calculated parameters for Eq. 9 and Eq. 11

| Shape of point on Figure | Grain size (nm) | Reciprocal cathodic over potential ($V^{-1}$) | $G_v$ $\mu m^3 * 10^9$ | Thickness of deposits (μm) | Time of deposition (s) | Ln [V $(G_v + A)^{-1}$] (Dimension less) | Current density (A $dm^{-2}$) | Cathode rotation speed (rpm) | Saccharin concentration (g $L^{-1}$) |
|---|---|---|---|---|---|---|---|---|---|
| Circle | 14 | 1.085 | 1,436 | 43 | 7,200 | 8.3328 | 2 | 500 | 5 |
| Lozenge | 18 | 1.1173 | 3,052 | 43.5 | 7,200 | 7.59063 | 2 | 600 | 5 |
| Lozenge | 20 | 1.1235 | 4,188 | 38 | 7,200 | 7.0567 | 2 | 300 | 5 |
| Circle | 23 | 1.1402 | 6,366 | 43.5 | 7,200 | 6.855 | 2 | 500 | 3 |
| Triangle | 27 | 1.1273 | 10,305 | 45 | 7,200 | 6.4077 | 2 | 0 | 5 |
| Circle | 28 | 1.1574 | 11,494 | 44.5 | 7,200 | 6.2886 | 2 | 500 | 1 |

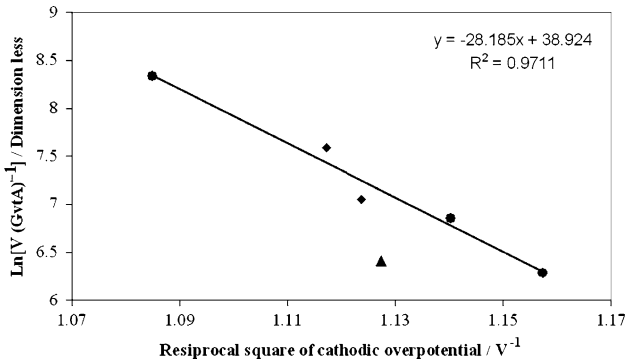


**Fig. 8** Graph of experimental data fitted to Eq. 9

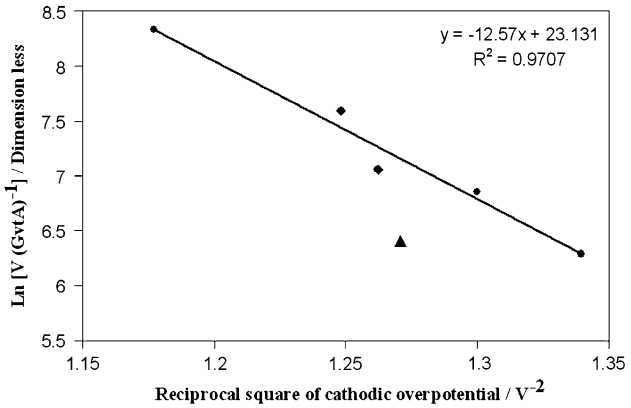


**Fig. 9** Graph of experimental data fitted to Eq. 11

adsorption which may change $bS\varepsilon^2$. In addition, the presence of concentration overpotential is probable for electrodeposition with a stationary cathode. Therefore, based on the Glasston relation [13], in spite of the high cathodic overpotential, the nucleation rate is smaller than that for deposition on the rotating electrode.

## 5 Conclusions

Nc nickel (14–28 nm) was electrodeposited with the combined advantages of using RCE and saccharin addition as a grain refiner from the Watts bath. Both cathode rotation speed and saccharin addition alter the grain size and cathodic overpotential. Results clearly indicate that using a RCE led to homogenous grain size and better saccharin adsorption on the cathode surface. At cathode rotation speeds of more than 500 rpm (saccharin concentration 5 g $L^{-1}$), in spite of greater inhibition to growth in the (100) direction, an increase in grain size and a decrease in absolute cathodic overpotential were observed. Therefore, the cathodic overpotential is more effective than inhibition of growth in the grain refining mechanism.

The electrodeposited grain size model accurately relates grain size to cathodic overpotential using a rotating cylindrical electrode at 2 A $dm^{-2}$. $Q_{2d}$ is about 28.185 V, the $k_{2d}$ is 8.02561 $\times$ $10^{16}$ $\mu m^{-2}s^{-1}$, $Q_{3d}$ is about 3.5454 V and $k_{3d}$ is 1.11087 $\times$ $10^{10}$ $\mu m^{-2}s^{-1}$. Deviation from the electrodeposition model is observed for a stationary cathode due to concentration overpotential. Therefore, it seems that only the activation part of the total overpotential plays an important role in decreasing the grain size. This is in good agreement with the change in composition of the Helmholtz layer as a result of saccharin adsorption that clearly changes the activation overpotential. The adverse effects of concentration overpotential which result from the increase in current density on the morphology of nickel deposits were also observed with SEM studies.

**Acknowledgements** The authors thank Shiraz University Research Council for financial support through grant number 84-GR-ENG-8. The valuable help of the laboratory staff of the Materials Science and Engineering Department in Shiraz University is greatly appreciated.

## References

1. Meyer MA, Mishra A, Benson DJ (2006) Prog Mater Sci 51:427
2. El-Sherik AM, Erb U (1995) J Mater Sci 50:5743
3. Erb U, El-Sherik AM (1994) US Patent # 5, 353, 266
4. Saber Kh, Koch CC, Fedkiw PS (2003) Mater Sci Eng A 341:174
5. Qiao G, Jing T, Wang N, Gao Y, Zhao X, Zhou J, Wang W (2005) Electrochim Acta 51:85
6. Lee KH, Chang D, Kwon SC (2005) Electrochim Acta 50:4538
7. Alfantazi AM, Erb U (1994) J Mater Sci Lett 15:1361
8. Wan CB, Wang DL, Chen WX, Wang YY (2002) Wear 253:563
9. Zimmerman AF, Palumbo G, Aust KT, Erb U (2002) Mater Sci Eng A 328:137
10. Erb U (1995) Nanostruct Mater 6:533
11. Choo RTC, Toguri JM, El-Sherik AM, Erb U (1995) J Appl Electrochem 25:384
12. Bockris JOM, Razumny GA (1967) Fundamental aspects of electrocrystallization. PlenumPress, NY, p 27
13. Glasstone S (1935) Trans Faraday Soc 31:1232
14. Roth CC, Leidheiser H (1953) J Electrochem Soc 100:553
15. Raub E, Baba N, Stalzer M (1964) Metalloberfache 18:323
16. Bonino JP, Pouderoux P, Rossignol C, Rousset A (1992) Plat Surf Finish 62:174
17. Saber Kh, Koch CC, Fedkiw PS (2003) Mater Sci Eng A 341:174
18. Natter H, Hempelmann R (1996) J Phys Chem 100:19525
19. Low CTJ, Wills RGA, Walsh FC (2006) Surf Coat Technol 201:371
20. Bahrololoom ME, Sani R (2005) Surf Coat Technol 192:154
21. Gabe DR, Wilcox GD, Gonzalez-Garcia J, Walsh FC (1998) J Appl Electrochem 28:759
22. Ebrahimi F, Bourne GR, Kelly MS, Matthews TE (1999) Nanostruct Mater 11(3):343
23. Lozano-Morales A, Podlaha EJ (2004) J Electrochem Soc 151(7):C478
24. Azaroff LV (1978) Elements of X-ray crystallography. McGraw Hill, 546 pp
25. Weil R, Cook HC (1962) J Electrochem Soc 109:295
26. Schuh CA, Nieh TG, Yamasaki T (2006) Scr Mater 46:735
27. Eisenberg M, Tobias CW, Wilke CR (1954) J Electrochem Soc 101:306
28. Erb U (1995) Nanostruct Mater 6:533

29. Mockute D, Bernotiene G, Vilkaite R (2002) Surf Coat Technol 160:152
30. Paunovic M, Schlesinger M (1998) Fundamentals of electrochemical deposition electrochemical society series. John Wiley and Sons Inc, New York, 53 pp
31. Crow DR (1994) Principles and applications of electrochemistry, 3rd edn. Chapman and Hall, 143 pp
32. Bercot P, Pena-Munoz E, Pagetti J (2002) Surf Coat Technol 157:282
33. Kim W, Weil R (1989) Surf Coat Technol 38:289
34. Wong KP, Chan KC, Yue TM (2001) Appl Surf Sci 178:178
35. Bozzini B (2000) Mater Chem Phys 66:278